Heliyon 10 (2024) e26904

Contents lists available at ScienceDirect

Heliyon

journal homepage: www.cell.com/heliyon

Research article

eIF2α-mediated integrated stress response links multiple intracellular signaling pathways to reprogram vascular smooth muscle cell fate in carotid artery plaque

Jichang Luo [a,b,1], Xiao Zhang [a,b,1], Wenjing Li [c,d,1], Tao Wang [a,b,1], Shengyan Cui [a,b], Tianhua Li [a,b], Yilin Wang [e], Wenlong Xu [a,b], Yan Ma [a,b], Bin Yang [a,b], Yumin Luo [e], Ge Yang [c,d,***], Ran Xu [a,b,**], Liqun Jiao [a,b,f,*]

[a] Department of Neurosurgery, Xuanwu Hospital, Capital Medical University, Beijing, China
[b] China International Neuroscience Institute (China-INI), Beijing, China
[c] Laboratory of Computational Biology and Machine Intelligence, National Laboratory of Pattern Recognition, Institute of Automation, Chinese Academy of Sciences, Beijing, China
[d] School of Artificial Intelligence, University of Chinese Academy of Sciences, Beijing, China
[e] Institute of Cerebrovascular Disease Research and Department of Neurology, Xuanwu Hospital of Capital Medical University, Beijing, China
[f] Department of Interventional Radiology, Xuanwu Hospital, Capital Medical University, Beijing, China

ARTICLE INFO

Keywords:
Carotid artery atherosclerosis
Primary vascular smooth muscle cells
Organelles
Plaque vulnerability
Translation initiation factor 2α

ABSTRACT

Background: Carotid arterial atherosclerotic stenosis is a well-recognized pathological basis of ischemic stroke; however, its underlying molecular mechanisms remain unknown. Vascular smooth muscle cells (VSMCs) play fundamental roles in the initiation and progression of atherosclerosis. Organelle dynamics have been reported to affect atherosclerosis development. However, the association between organelle dynamics and various cellular stresses in atherosclerotic progression remain ambiguous.

Methods: In this study, we conducted transcriptomics and bioinformatics analyses of stable and vulnerable carotid plaques. Primary VSMCs were isolated from carotid plaques and subjected to histopathological staining to determine their expression profiles. Endoplasmic reticulum (ER), mitochondria, and lysosome dynamics were observed in primary VSMCs and VSMC cell lines using live-cell imaging. Moreover, the mechanisms underlying disordered organelle dynamics were investigated using comprehensive biological approaches.

Results: ER whorls, a representative structural change under ER stress, are prominent dynamic reconstructions of VSMCs between vulnerable and stable plaques, followed by fragmented mitochondria and enlarged lysosomes, suggesting mitochondrial stress and lysosomal defects, respectively. Induction of mitochondrial stress alleviated ER stress and autophagy in an eukaryotic translation initiation factor (eIF)-2α-dependent manner. Furthermore, the effects of eIF2α on ER stress, mitochondrial stress, and lysosomal defects were validated using clinical samples.

* Corresponding author. Department of Neurosurgery, Xuanwu Hospital, Capital Medical University, Beijing, China.
** Corresponding author. Department of Neurosurgery, Xuanwu Hospital, Capital Medical University, Beijing, China.
*** Corresponding author. Laboratory of Computational Biology and Machine Intelligence, National Laboratory of Pattern Recognition, Institute of Automation, Chinese Academy of Sciences, Beijing, China.
E-mail addresses: ge.yang@ia.ac.cn (G. Yang), xrqssq@126.com (R. Xu), liqunjiao@sina.cn (L. Jiao).
[1] These authors contributed equally.

https://doi.org/10.1016/j.heliyon.2024.e26904
Received 1 October 2023; Received in revised form 14 February 2024; Accepted 21 February 2024
Available online 23 February 2024

Conclusion: Our results indicate that morphological and functional changes in VSMC organelles, especially in ER whorls, can be used as reliable biomarkers for atherosclerotic progression. Moreover, eIF2α plays an important role in integrating multiple stress-signaling pathways to determine the behavior and fate of VSMCs.

Abbreviations and acronyms

VSMCs	Vascular Smooth Muscle Cells
PVSMC(S)	Primary Vascular Smooth Muscle Cells Derived From Stable Plaques
PVSMC(V)	Primary Vascular Smooth Muscle Cells Derived From Vulnerable Plaques
HA-VSMC	Human Aortic Vascular Smooth Muscle Cell
HC-VSMC	Human Carotid Vascular Smooth Muscle Cell
HG	High Glucose
ox-LDL	Oxidative Low-Density Lipoprotein
UPR	Unfolded Protein Response
ROS	Reactive Oxygen Species
ER	Endoplasmic Reticulum
PERK	Protein Kinase RNA-Like Endoplasmic Reticulum Kinase
XBP1	X-Box Binding Protein 1
DRP1	Dynamin-Related Protein 1
p-DRP1 (S616)	Phospho-Dynamin-Related Protein 1(Ser 616)
Tom 20	Translocase Of Outer Membrane 20
LAMP1	Lysosomal-Associated Membrane Protein 1
LC3	Light Chain 3
α-SMA	Alpha-Smooth Muscle Actin
MMP2	Matrix Metallopeptidase 2
GFP	Green Fluorescent Protein
DTT	Dithiothreitol
eIF2α	Eukaryotic Translation Initiation Factor 2α
ALDH2	Enzyme Aldehyde Dehydrogenase 2
GRP 78	Glucose-Regulated Protein 78
ISR	Integrated Stress Responses

1. Background

Carotid arterial atherosclerotic stenosis is a major cause of ischemic stroke, accounting for approximately 15% of all strokes worldwide recently [2]. Plaque vulnerability is the main factor in the pathogenesis of carotid artery stenosis, which results in plaque rupture and rapid thrombosis [3,4]. Plaque vulnerability is determined by the thickness of the fibrous cap and the size of atheroma contents, and vascular smooth muscle cells (VSMCs) play an essential role in this process [5,6]. Therefore, altered behaviors of VSMCs, such as decreased migration and proliferation and excessive apoptosis, may increase plaque vulnerability.

Organelles, such as the endoplasmic reticulum (ER), mitochondria, and lysosomes, are vital for metabolic homeostasis involving the synthesis and modification of proteins, energy metabolism, and cellular degradation [7–9]. Morphological changes in organelles, such as ER whorls, fragmented mitochondria, and enlarged lysosomes, are regulated by complicated molecular signaling pathways and associated with multiple cellular stresses, including ER stress, mitochondrial stress, and lysosomal defects [10–13]. Accumulating evidence has demonstrated that cellular stress is closely related to metabolic disorders and inflammatory reactions in atherosclerosis, which may be the underlying cause of plaque vulnerability [14]. However, the specific association between the organelle dynamics of VSMCs and multiple cellular stresses and atherosclerosis progression as well as the underlying mechanisms remain unclear.

Eukaryotic translation initiation factor (eIF)-2α is phosphorylated by protein kinase RNA-like ER kinase (PERK) under ER stress and is involved in the initiation and development of atherosclerosis by regulating translation and protein synthesis [15]. Elevated eIF2α expression is a protective mechanism for relieving atherosclerosis progression [16]. eIF2α is also suggested to mediate the integrated stress response (ISR). Its phosphorylation is controlled by multiple stress-related pathways, such as ER stress, reactive oxygen species, nitric oxide, and amino acid deficiency, and it contributes to protein and energy homeostasis [17]. Regardless of the pathogenetic significance of multiple cellular stresses in atherosclerosis, the role of eIF2α in atherosclerosis from the perspective of ISR remains unknown.

In this study, we aimed to explore the association between organelle dynamics and various cellular stresses in atherosclerotic procession, and clarify the potential mechanism of eIF2α for regulating the behavior and cell fate of VSMCs during atherosclerosis.

2. Materials and methods

2.1. Ethics statement

This study was approved by the Ethics Committee of Xuanwu Hospital, Capital Medical University (KS2021124-1). The human research conducted in this study adhered to the principles outlined in the Declaration of Helsinki (revision 6, 2008) and was executed in accordance with institutional guidelines. Informed consent was obtained from all patients who underwent carotid endarterectomy and provided specimens for this study.

2.1.1. Specimen collection

A total of 40 carotid plaques were obtained from patients with asymptomatic or symptomatic high-grade carotid artery stenosis (>50% for symptomatic and >70% for asymptomatic patients according to the North American Symptomatic Carotid Endarterectomy Trial criteria for carotid stenosis) [18] at Xuanwu Hospital, Capital Medical University between July 2020 and December 2021. Only the diseased portion was removed during surgery. Patients with re-stenotic lesions following carotid endarterectomy were excluded from the study. The plaque was divided longitudinally along the vessel axis; half was used for the culture of primary VSMCs and the other half was fixed in 4% Zn-formaldehyde and processed for histopathology. Plaques were classified into stable and vulnerable types based on ultrasound and histopathological findings. Vulnerable plaques are characterized by intraplaque hemorrhage, mural thrombus, thin fibrous caps, or an incomplete fibrous cap, otherwise they are known as stable plaques [19]. Thirty plaques were used to isolate and culture primary VSMCs for histological examination. Ten plaques, five of which were stable and five were unstable, were processed for the transcriptomic assay.

2.2. Isolation and culture of primary VSMCs

Plaques separated from patients were immediately stored in sterile phosphate-buffered saline (PBS, 0.01 mol/L, pH 7.4) on ice and transferred to the laboratory within 3 h. They were isolated, divided into several pieces of 2–3 mm^2, washed with PBS (0.01 mol/L, pH 7.4), and plated on culture dishes coated with 0.1% gelatin in an SmGM2 human smooth muscle growth medium (Lonza; medium containing 5% serum, epidermal growth factor, fibroblast growth factor-2, insulin, and antibiotics). The medium was changed seven days after planting and every three days thereafter. After 2–3 weeks, the cells were observed on the plate. As the cells became dense, the pieces were removed, and the cells were passed at a 1:2 ratio. Primary VSMCs from plaques were cultured in the SmGM2 human smooth muscle growth medium (Lonza) and investigated between the second and fourth passages.

2.3. Plaque histopathology, immunohistochemistry (IHC), and immunofluorescence (IF) staining

IHC and IF microscopy for VSMCs were performed, as previously described [20]. Representative specimens of stable and vulnerable plaques were fixed in 4% buffered formalin and embedded in paraffin. Sections, each 5 μm thick, were stained with hematoxylin and eosin and Masson's trichrome stain. Immunoreactivity was enhanced via microwave treatment (750 W, 16 min) in citrate buffer (10 mmol/L, pH 6.0). IF for anti-α-smooth muscle actin (α-SMA; 1A4, mouse, 1:200; Cell Signaling Technology) and antimatrix metalloproteinase 2 (MMP2; rabbit, 1:400; D4M2N) was conducted on adjacent sections of plaques. IHC for α-SMA (1A4, mouse, 1:300; Cell Signaling Technology), anti-PERK (D11A8; Cell Signaling Technology), X-box-binding protein 1 (XBP1; 102256-T34; Sino Biological Inc.), anti-cytochrome C (ab133504; Abcam), anti-lysosomal-associated membrane protein 1 (LAMP1; 21997-1-AP; Proteintech), and anti-eIF2α (11170-1-AP; Proteintech) was also performed on adjacent plaque sections. All assays were performed according to the protocol of the Immunostimer LabVision Autostainer 720 (Thermo Scientific) with the UltraVision Quanto HRP DAB [21]. The stained images were captured at × 200 and × 400. In each slice, all fields of view of the plaque were examined and five different random positions were selected for expression scores.

IF staining of primary VSMCs was performed using the same antibodies. Briefly, the cells were fixed with 4% paraformaldehyde for 20 min and permeabilized with PBS containing 1% Triton X-100 (PBST). After washing thrice with PBST, cells were incubated with anti-SMA and anti-MMP2 at room temperature (20 °C) for 4 h. Alexa 488-conjugated goat anti-rabbit IgM and Rhodamine-conjugated goat anti-mouse IgM were used as the secondary antibodies. Nuclei were stained with Hoechst 33258 (94403; Sigma-Aldrich).

2.4. Establishment of the VSMC culture

Established VSMCs, including human aortic VSMCs (HA-VSMCs) and human carotid VSMCs (HC-VSMCs), were purchased from Bluefbio (www.bluefcell.com) and cultured in high-glucose (HG)-containing Dulbecco's modified Eagle's medium (normal glucose: 5.5 mM; SH30022.01; Hyclone) supplemented with 10% fetal bovine serum (FBS; 10099-141; Gibco-Invitrogen) at 37 °C in 5% CO_2. Cells were passaged at a ratio of 1:3 to 1:6, and the culture medium was changed every three days.

2.4.1. Fluorescent labeling

Both primary and established VSMCs were labeled using the same protocol. To fluorescently label the ER, cells were infected with GFP-sec61β lentivirus supplied with 8–10 μg/mL polybrene. Viruses were removed 24–36 h after infection. To label the mitochondria and lysosomes, cells were incubated with 50 nM MitoTracker Deep Red FM (M2242; ThermoFisher Scientific) and 0.5 mg/mL Dextran Alexa Fluor 647 (D22914; ThermoFisher Scientific) solution, respectively. After 15–45 min, the staining solution was replaced with

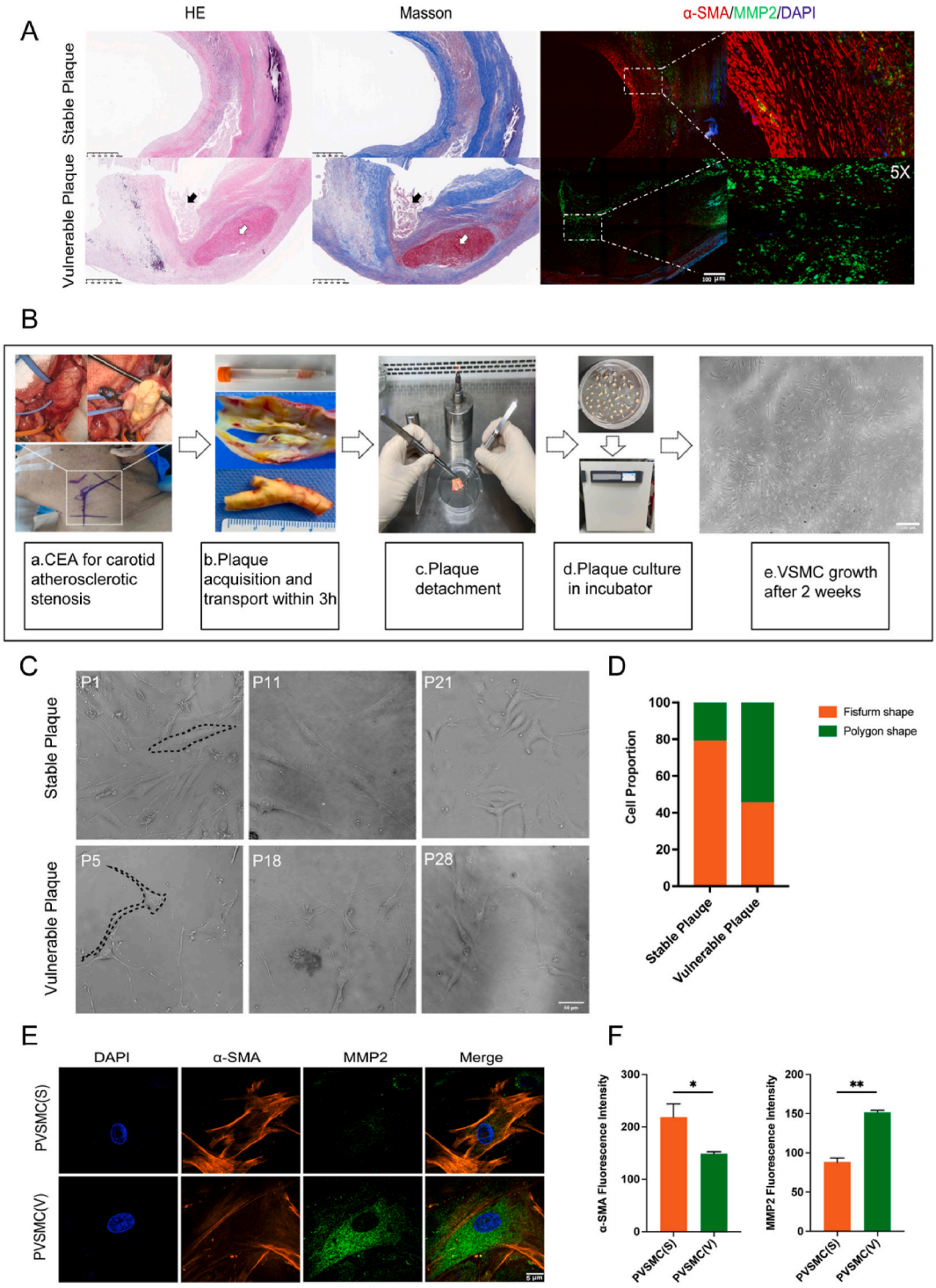

Fig. 1. Cultivation of primary vascular smooth muscle cells (VSMCs) from stable and vulnerable plaques. **(A)** Hematoxylin and eosin (H&E), Masson's trichome, and immunofluorescence staining of α-smooth muscle actin (α-SMA) and matrix metalloproteinase 2 (MMP2) for histopathology of stable and vulnerable plaques. **(B)** Isolation and cultivation of primary VSMCs from human carotid plaques. **(C)** Morphology of primary VSMCs from stable and vulnerable plaques. **(D)** Quantitative analysis of cell proportions of fusiform and polygonal VSMCs derived from stable and vulnerable plaques (n = 15 patients in each group). **(E)** Immunofluorescence staining of primary VSMCs from stable and vulnerable plaques with α-SMA and MMP2. **(F)** Quantitative analysis of the fluorescence intensities of α-SMA and MMP2 in primary VSMCs from stable and vulnerable plaques (n = 30 cells in each group). *p < 0.05 and **p < 0.01 vs. PVSMC(S). *p < 0.05 and **p < 0.01.

fresh prewarmed media and live-cell imaging was performed.

2.4.2. Pharmacological treatments

Established VSMCs were treated with 3 mM dithiothreitol (DTT; HY-15917; MedChemExpress), 1 μM oligomycin A (HY-16589; MedChemExpress), 1 μM bafilomycin A_1 (HY-100558; MedChemExpress) for 24 h to evaluate the morphological changes in the ER, mitochondria, and lysosomes, respectively. Additionally, established VSMCs were treated with maximal concentrations of high glucose (20 mM; G7021; Sigma) and oxidized low-density lipoprotein (ox-LDL; 50 μg/mL; YB-002; Yiyuan Biotechnology) for 24h to mimic the atherosclerotic environment, as previously described [22,23]. Furthermore, in the verification test, 5 μM thapsigargin (Tg; HY-13433; MedChemExpress) was used to induce ER stress, and 100 nM ISRIB (HY-12495; MedChemExpress) was used to inhibit the phosphorylation of eIF2α in VSMCs. When multiple drugs are required to be treated together, we mixed the same concentration of drugs together to treat the established VSMCs for 24h.

2.4.3. Western blotting

Western blotting was performed to confirm the induction of ER stress, mitochondrial stress, and lysosomal defects. Cell proteins (20 μg) were loaded onto a 4–12% polyacrylamide gel and separated via electrophoresis. Proteins were transferred to polyvinylidene fluoride membranes, blocked in 5% skin milk for 0.5 h, and incubated with the following primary antibodies: anti-PERK(D11A8; Cell Signaling Technology), anti-actin (BE0021-100; Easybio), anti-XBP1 (102256-T34; Sino Biological Inc.), anti-DRP1 (D6C7; Cell Signaling Technology), anti-phospho-DRP1 (Ser616) (pDrp1 (S616)) (D9A1; Cell Signaling Technology), anti-Tom 20 (D8T4N; Cell Signaling Technology), anti-light chain 3 (LC3; 14322-T44; Sino Biological Inc.), anti-LAMP1 (21997-1-AP; Proteintech), anti-GRP78 (HG12063-UT; Sino Biological Inc.), and anti-eIF2α (11170-1-AP; Proteintech) antibodies. For the quantitative analysis of western blotting, we used Fuji software to measure the average gray value of the strips and obtained a homogenized ratio compared with the gray value of the strips in the internal reference, and then performed statistical analysis by the magnitude of the ratio.

2.4.4. Fluorescence microscopy

Cells were grown on cover-glass MatTek dishes at 60% confluency. After incubation in the imaging dish for more than 24 h, images were taken using a TI2-E inverted microscope (NIKON) equipped with a 100 × 1.45-N. A. oil objective, 405/488/561/647 nm lines of a laser system (Oxxis), a CSUW1 Spinning Disk scan head (Yokogawa), and a 95BSI sCMOS camera (PRIME). The hardware was driven by Nikon Elements (Nikon). During imaging, the cells were kept in an incubator at 37 °C and 5% CO_2 (Tokai heat) for time-lapse imaging.

2.5. Quantification and statistical analysis

Image quantification was performed using the Fiji (https://imagej.net/software/fiji/). Plugins of "Mitochondria Analyzer" and "3D object counter" were used to quantify the shape and number of mitochondria and lysosomes, respectively. We used analysis of variance (ANOVA) to compare more than two groups. Student's *t*-test or Mann-Whitney *U* test was used to examine statistical differences between two groups. Categorical data was analyzed using $\chi 2$ tests and Fisher's exact tests. The analysis was conducted using GraphPad Prism version 9.00 (GraphPad, La Jolla, CA, USA). Statistics were considered significant when P-values <0.05 were involved.

3. Results

3.1. Cultivation of primary VSMCs from stable and vulnerable plaques

The content and phenotype of VSMCs is an important factor for determining plaque stability. Plaques with thin fibrous caps, intraplaque hemorrhage, and plaque rupture were selected as representative vulnerable plaques, whereas those with thick fibrous caps were taken as representative stable plaques [24]. Molecular markers of α-SMA, a marker of contractile VSMCs, and MMP2, a marker of synthetic VSMCs, are specific to the VSMC subtype. We performed *in situ* immunofluorescent staining of these molecular markers between stable and vulnerable human plaques obtained by carotid endarterectomy in patients with atherosclerotic carotid artery stenosis, which showed that *in situ* VSMCs had higher expression of α-SMA and lower levels of MMP 2 (contractile VSMCs) in stable plaques, and vice versa in vulnerable plaques (synthetic VSMCs) (Fig. 1A). To explore the corresponding shifts during alterations of VSMC phenotype, primary VSMCs were isolated and cultured from human plaques, which were visible 2 weeks after explant (Fig. 1B). Primary VSMCs derived from stable and vulnerable plaques showed morphological differences (Fig. 1C). VSMCs derived from stable plaques are referred to as PVSMC(S), whereas those derived from vulnerable plaques are referred to as PVSMC(V). Approximately 80% of the PVSMC(S) exhibited fusiform shapes, whereas 60% of the PVSMC(V) presented polygonal shapes with long tentacles (Fig. 1C and D). In addition, immunofluorescence staining showed a significant difference between PVSMC(V) and PVSMC(S) with respect to the expression levels of α-SMA and MMP2, in which PVSMC(S) exhibited high expression of α-SMA and low expression of MMP2, whereas PVSMC(V) exhibited the opposite expression pattern (Fig. 1E and F) ($p < 0.01$). The results from **primary VSMCs** confirmed that plaque vulnerability is associated with the phenotypic properties of VSMCs.

Characterizing cellular organelle changes in human VSMCs that play a key roles in plaque vulnerability.

To explore the corresponding shifts of gene expression regulation in VSMC phenotype switch. We collected five representative stable and five representative vulnerable plaques to conduct a RNA-seq assay, which reveals the changes in the transcriptome of stable and vulnerable plaques. Using gene expression data from the Gene Expression Omnibus database (http://www.ncbi.nlm.nih.gov/geo/

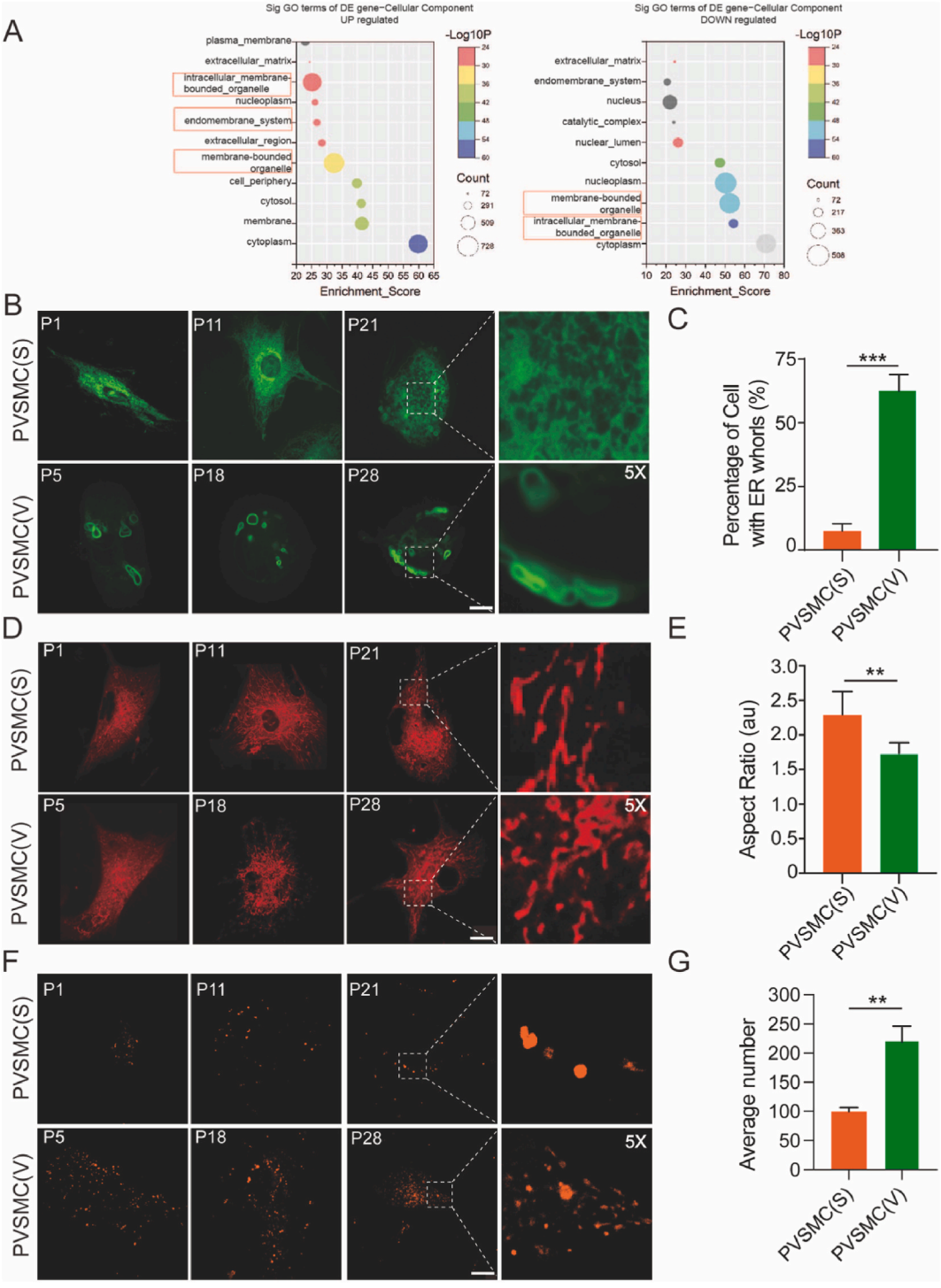

(caption on next page)

Fig. 2. Increased endoplasmic reticulum (ER) whorls, fragmented mitochondria, and enlarged lysosomes in VSMCs derived from vulnerable plaques (PVSMC(V)) than in those derived from stable plaques (PVSMC(S)). **(A)** Bioinformatics analysis to identify differentially expressed genes between stable and vulnerable plaques. **(B)** Representative image of endoplasmic reticulum (ER) labeled with GFP-Sec61β in PVSMC(S) and PVSMC(V). **(C)** Quantitative analysis of the percentage of cells with ER whorls in the two groups (n = 30 cells in each group). **(D)** Representative image of mitochondria stained with deep red Mitotracker in PVSMC(S) and PVSMC(V). **(E)** Quantitative analysis of the aspect ratio in the two groups (n = 30 cells in each group). **(F)** Representative image of lysosomes stained with dextran in PVSMC(S) and PVSMC(V). **(G)** Quantitative analysis of the average number of lysosomes in the two groups (n = 30 cells each). **p < 0.01 and ***p < 0.001. Scale bar = 10 μm. P1, P11, P21, P5, P18, P28 refer to the corresponding patient plaque numbers. (For interpretation of the references to colour in this figure legend, the reader is referred to the Web version of this article.)

), we found differences in the intracellular membrane-bounded organelles, endomembrane systems, and membrane-bound organelles between stable and vulnerable plaques (Fig. 2A). 1112 and 640 of the total 17131 genes were significantly upregulated and down-regulated in (fold change >1.5 and adjusted P < 0.05) in vulnerable plaque, compared with stable one, respectively. Genes with upregulated were highly enriched in the term 'in cellularmembrane bounded organelles'(-log10p = 25.18, count = 673). Additionally,'endomembrane_system' (-log10p = 26.72, count = 270) and 'membrane bounded organelle' (-log10p = 32.32,count = 728) related genes were also significantly upregulated. Similarly, 'endomembrane_system'(-log0p = 20.54,count = 176) and 'membrane-bounded organelle' (-log0p = 50.28,count = 508) related genes were down-regulated in vulnerable plaques compared with stable plaques (Fig. 2A).

Due to the pivotal role of VSMCs in plaque stability, we decided to investigate whether organelle dynamics are altered in primary VSMCs from various types of plaques. Multiple organelles, including the ER, mitochondria, lysosomes, and nucleus, were simultaneously illuminated and their dynamic morphological changes were monitored (Supplementary Fig. 1A and 1B). ER networks, labeled with GFP-fused ER membrane-located Sec61 transposon complex subunit β (Sec61 β), constantly change their shape. Mitochondria undergo a fusion-fission cycle, lysosomes undergo rapid movement, and their size changes continuously. Abnormal organelle morphology has also been observed in PVSMCs. ER whorls, characterized by multiple layers of concentric layers, show a ring-shaped pattern and contribute to translational inhibition and compartmentalization of unfolded proteins to counterbalance ER stress [25–27]. We observed that the percentage of cells with ER whorls in PVSMC(V) was higher than that in PVSMC(S) (p < 0.001) (Fig. 2B and C), and the increased ER whorl percentage in PVSMC(V) indicated elevated levels of ER stress during plaque progression. The shape and size of the mitochondria are characterized by alternating cycles of fission and fusion of organelles. Fragmented mitochondria indicate increased mitochondrial fission in response to mitochondrial stress during atherosclerosis [28]. Mitochondrial fission decreased the mitochondrial aspect ratio, area, perimeter, and branch length, which coincided with the mitochondrial features in PVSMC(V) compared with PVSMC(S) with a reduced aspect ratio (1.74 vs. 2.3; p < 0.01) (Fig. 2D and E), as well as the average area (0.35 vs. 0.62 μm^2; p < 0.01), perimeter (2.41 vs. 3.78 μm; p < 0.01), and branch length (0.71 vs. 1.03 μm; p < 0.01) (Supplementary Figure 1). Lysosomes are organelles that can degrade endogenous and exogenous substrates [29]. In atherosclerosis, lysosomes play a significant role in handling lipoproteins, processing autophagy, and regulating multiple signaling pathways, such as mTOR [30,31]. Lysosomes were stained with dextran and imaged using spinning disk confocal microscopy. There were significant differences in the average number of lysosomes (222.1 vs. 99.4/cell; p < 0.01) between the PVSMC(V) and PVSMC(S) (Fig. 2F and G). As the increased size and number of lysosomes represent lysosomal dysfunction, enlarged lysosomes in PVSMC(V) may imply lysosomal defects during atherosclerotic progression [32]. All these data suggest that the impaired biological process in VSMCs involves multiple cellular organelles, which is distinguishable cellular changes between vulnerable plaques compared with the stable one.

3.2. Morphological changes in organelles and corresponding cellular stress responses caused by atherosclerotic stimulation in cultured VSMCs

High blood glucose and ox-LDL cholesterol levels were assessed as independent risk factors for plaque vulnerability [33,34]. We analyzed the clinical information of the patients used for culturing primary VSMCs. We found that ox-LDL and blood glucose levels were higher in patients with vulnerable plaques than in those with stable plaques (p < 0.0001) (Supplementary Table 1). To mimic the physiological conditions of hyperglycemia and hyperlipidemia, established HA-VSMCs and HC-VSMCs were treated with the atherosclerotic stimulators HG and ox-LDL. Typical cellular stress-related components, such as DTT (ER stress inducer), oligomycin A (mitochondrial stress inducer), and bafilomycin A_1 (degradation inhibitor), were also used as positive controls. Compared to primary VSMCs, atherosclerotic stimulation resulted in a similar organelle phenotype. HG and ox-LDL treatment led to a higher percentage of ER whorl formation in HA-VSMCs than in the control treatment as well as in HC-VSMCs (both p < 0.001) (Fig. 3A and B). Western blotting results revealed that ER whorl formation was accompanied by activation of the unfolded protein response (UPR) signaling pathway. The expression levels of PERK (Protein Kinase RNA-like Endoplasmic Reticulum Kinase), a branch pathway of UPR, were increased in HG and ox-LDL treatment, and enhanced splicing of XBP1 (IRE1α branch of UPR) was also detected in HA-VSMCs and HC-VSMCs treated with HG and ox-LDL (Fig. 3C; Supplementary Figure 2A). All findings caused by HG and ox-LDL were similar to the results induced by DTT (dithiothreitol), which triggers protein misfolding and aggregation by disrupting disulfide bonds (Fig. 3A, B, 3C). Thus, HG and ox-LDL trigger the ER stress and cause ER whorl deformation.

Mitochondria are energy-producing organelles that utilize glucose and lipid for energy production, and their dynamic shape is sensitive to the environmental glucose and lipid concentration [22,23]. We observed that HG and ox-LDL induced mitochondrial fission in both HA-VSMCs and HC-VSMCs with less aspect ratio (1.73 vs. 1.61 and 1.81 vs. 1.61, respectively; p < 0.05), area (0.47 vs. 0.39 μm^2 and 0.51 vs. 0.39 μm^2, respectively; p < 0.05), perimeter (2.75 vs. 2.21 μm and 2.86 vs. 2.21 μm, respectively; p < 0.01), and

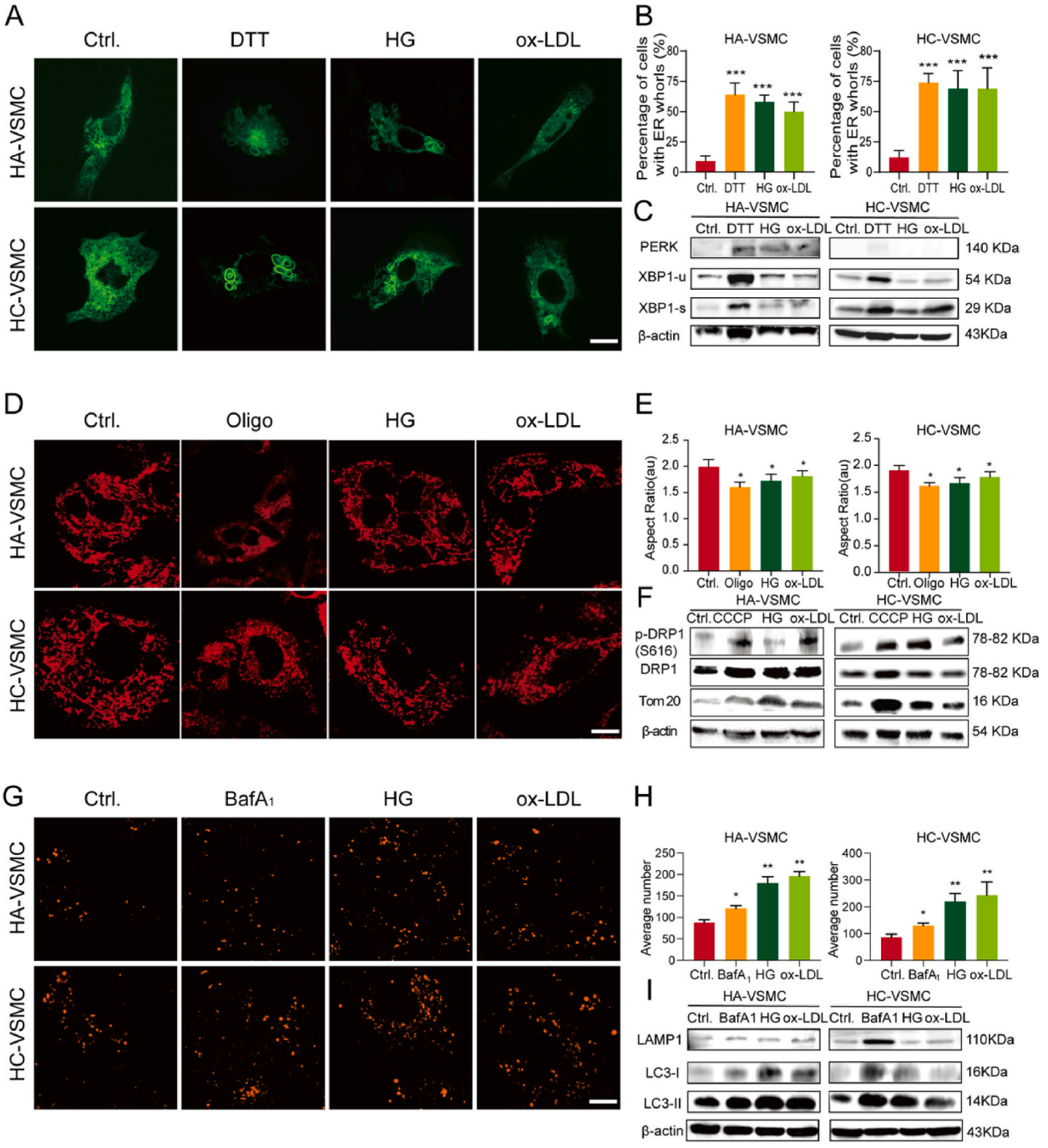

(caption on next page)

Fig. 3. Morphological changes in organelles under atherosclerotic stimulations with high glucose (HG) and oxidized low-density lipoprotein (ox-LDL) are associated with cellular stress responses. **(A)** Representative image of ER labeled with GFP-Sec61β in human aortic VSMCs (HA-VSMCs) and human carotid VSMCs (HC-VSMCs) treated with dimethyl sulfoxide (DMSO; control group, Ctrl.), dithiothreitol (DTT; 3 mM), HG (20 mM), and ox-LDL (50 μg/mL) for 24 h. **(B)** Quantitative analysis of the percentage of cells with ER whorls in HA-VSMCs and HC-VSMCs treated with DMSO, DTT, HG, and ox-LDL (n = 30 cells in each group). **(C)** Western blotting analysis of PERK, spliced X-box-binding protein 1 (XBP1-s) and unspliced XBP1 (XBP1-u) in HA-VSMCs and HC-VSMCs treated with DMSO, DTT, HG, and ox-LDL (n = 3 times each group). **(D)** Representative image of mitochondria stained with deep red Mitotracker in HA-VSMCs and HC-VSMCs treated with DMSO (Ctrl.), oligomycin A1 (Oligo, 1 μM), HG (20 mM), and ox-LDL (50 μg/mL) for 24 h. **(E)** Quantitative analysis of the aspect ratio in HA-VSMCs and HC-VSMCs treated with DMSO, Oligo, HG, and ox-LDL (n = 30 cells in each group). **(F)** Western blotting analysis of p-DRP1(S616), DRP1, and Tom 20 proteins in HA-VSMCs and HC-VSMCs treated with DMSO, Oligo, HG, and ox-LDL (n = 3 times each group). **(G)** Representative image of lysosomes stained with dextran in HA-VSMCs and HC-VSMCs treated with DMSO (Ctrl.), bafilomycin A1 ($BafA_1$, 1 μM), HG (20 mM), and ox-LDL (50 μg/mL) for 24 h. **(H)** Quantitative analysis of the changes in the number and fluorescence intensity of lysosomes in HA-VSMCs and HC-VSMCs treated with DMSO, $BafA_1$, HG, and ox-LDL (n = 30 cells in each group). **(I)** Western blotting analysis of lysosomal-associated membrane protein 1 (LAMP1), light chain 3 (LC3)-1, and LC3-II in HA-VSMCs and HC-VSMCs treated with DMSO, $BafA_1$, HG, and ox-LDL (n = 3 times each group). *p < 0.05, **p < 0.01, and ***p < 0.001. Scale bar = 10 μm. (For interpretation of the references to colour in this figure legend, the reader is referred to the Web version of this article.)

branch length (0.58 vs. 0.43 μm and 0.65 vs. 0.43 μm, respectively; $p < 0.05$) (Fig. 3D and E; Supplementary Figure 2B). We investigated whether fragmented mitochondria in VSMCs were a consequence of the activation of mitochondrial fission-related signaling. Using Western blot analysis, we determined that mitochondrial fission-related proteins, such as DRP1, p-DRP1(S616), and Tom20, were all expressed in HA-VSMCs and HV-VSMCs. Consistent with elevated mitochondrial fission, Tom 20 and p-DRP1(S616) were upregulated when cells were treated with HG and ox-LDL (Fig. 3F; Supplementary Figure 2B). Both imaging and western blotting assays revealed that enhanced mitochondrial fission caused by HG and ox-LDL was similar to the results induced by oligomycin A, an inhibitor of H^+-ATP synthase promoting mitochondrial fission and mitochondrial stress [35] (Fig. 3D, E, 3F). Similar to oligomycin A, HG and ox-LDL induce upregulated mitochondrial fission mediated by the phosphorylated DRP1 machinery.

Lastly, it has been demonstrated that HG and ox-LDL alkalize lysosomal pH, impair the degradation capacity of lysosomal hydrolases, and cause damage to the lysosomal membrane [36]. We also tested the behavior of lysosomes in VSMCs during the development of atherosclerosis. We found that both HG and ox-LDL treatment increased the average number of lysosomes per cell (180.1 vs. 88.7 and 196.6 vs. 88.7, respectively; $p < 0.01$) in HA-VSMCs and HC-VSMCs (Fig. 3G and H). To determine whether lysosomal membrane integrity and autophagy signaling were associated with morphological changes in lysosomes, markers, such as LAMP1, LC3I, and LC3II proteins, were detected by western blotting. Expression levels of LAMP-1, LC3I, and LC3II increased after treatment, suggesting that the membrane integrity and autophagy function of lysosomes were impaired (Fig. 3I; Supplementary Figure 2C). Moreover, all the findings caused by HG and ox-LDL were similar to those induced by bafilomycin A_1 ($BafA_1$), a degradation and autophagy inhibitor [37] (Fig. 3G, H, 3I), indicating that both HG and Ox-LDL cause lysosomal defects by damaging membrane integrity and inhibiting autophagy function. Therefore, atherosclerotic stimulations such as HG and Ox-LDL, critical factors for plaque vulnerability, lead to cellular stress responses and morphological changes of organelles.

3.3. Multiple cellular stress responses are associated with plaque vulnerability

Given that the multiple cellular stress responses are observed in VSMCs, we have validated whether they function in plaque vulnerability using clinical samples. Thirty carotid atherosclerotic plaques from 30 patients who underwent carotid endarterectomy were used in this study. There were 15 patients each in the stable and vulnerable plaque groups. IHC was performed for α-SMA (VSMC viability), PERK, XBP1, GRP 78 (ER stress), cytochrome C (mitochondrial stress), LAMP1 (lysosome membrane integrity), and eIF2α (ISR) on adjacent sections of plaques in each case. The low expression of α-SMA indicated a low content of VSMCs, representing vulnerable plaques, which was verified by the findings of HE (Fig. 4A and B). Consistent with the transcriptome data and primary VSMC observations, the expression of ER stress-related genes, *XBP1* and *GRP78*, was more prominent in the vulnerable plaque group than in the stable plaque group (n = 30, $p < 0.001$), while the mitochondrial stress marker, cytochrome C, and lysosomal marker, LAMP1, were differentially expressed with small differences (n = 30, $p < 0.05$), and no differences in PERK expression were observed between the stable and unstable plaque groups (Fig. 4A and B). Notably, eIF2α levels were dramatically elevated in the vulnerable group independent of PERK ($p < 0.01$), implying the important role of eIF2α mediated ISR but not ER stress only in plaque vulnerability.

3.4. eIF2α-mediated ISR is involved in the regulation of atherosclerotic plaque progression

To explore the potential mechanisms underlying multiple stressors co-exist and contribute to plaque vulnerability, cultured HC-VSMCs were stimulated either/both with Tg (ER stress inducer) and oligo (mitochondrial stress inducer) to mimic the multiple stress enviroument during atherosclerotic plaque progression. Perticularly, morphological markers including ER whorls, fragmented mitochondria, and enlarged lysosomes together with Western blot assay are used for quantifying cell stress levels. Tg and/or oligo treatment caused similar fragmented mitochondrial phenotypes (Fig. 5A and B), but showed different activity in ER whorl regulation. Oligomycin A supplementation rescued the ER whorl phenotype caused by Tg, although oligomycin A alone did not induce ER whorl formation (Fig. 5A and B). Western blotting also revealed that the ER stress-induced expression of eIF2α was inhibited by oligomycin A-induced mitochondrial stress (Fig. 5E; Supplementary Figure 2D). The same tendency was also found for other ER stress markers GRP

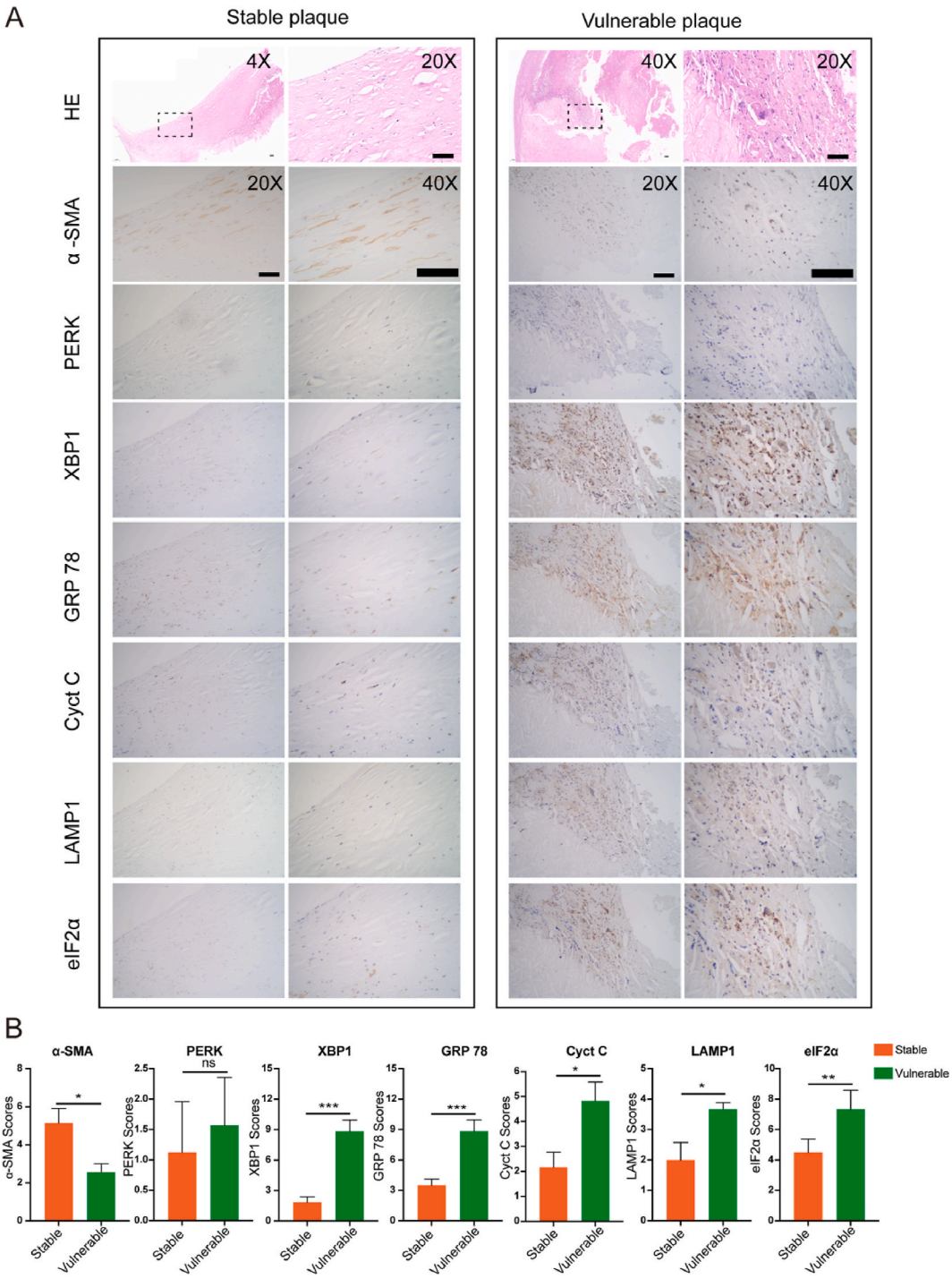

Fig. 4. eIF2α-mediated integrated stress responses verified in carotid stable and vulnerable plaques. **(A)** Representative specimens of stable and vulnerable plaques stained with H&E, and immunohistochemistry (IHC) of VSMCs with organelle markers, including α-SMA, PERK, XBP1, GRP78, cytochrome C (Cyt C), LAMP1, and eIF2α. **(B)** Quantitative analysis of the expression levels of α-SMA, PERK, XBP1, GRP78, Cyt C, LAMP1, and eIF2α (n = 15 cases in each group). *p < 0.05, **p < 0.01, and ***p < 0.001. Scale bar = 200 μm, 1 cm, 2 cm, respectively.

78 and spliced XBP1 (Fig. 5E; Supplementary Figure 2D). Interestingly, although both ER stress and mitochondrial stress triggered autophagy, as indicated by the LC3I level, double treatment completely blocked autophagy (Fig. 5E; Supplementary Figure 2D). These findings imply that mitochondrial stress could relieve ER stress, and their balance is crucial for determining the fate of VSMCs.

Previous studies have reported that eIF2α, a critical protein that catalyzes the initiation of protein synthesis, is involved in ISR [41].

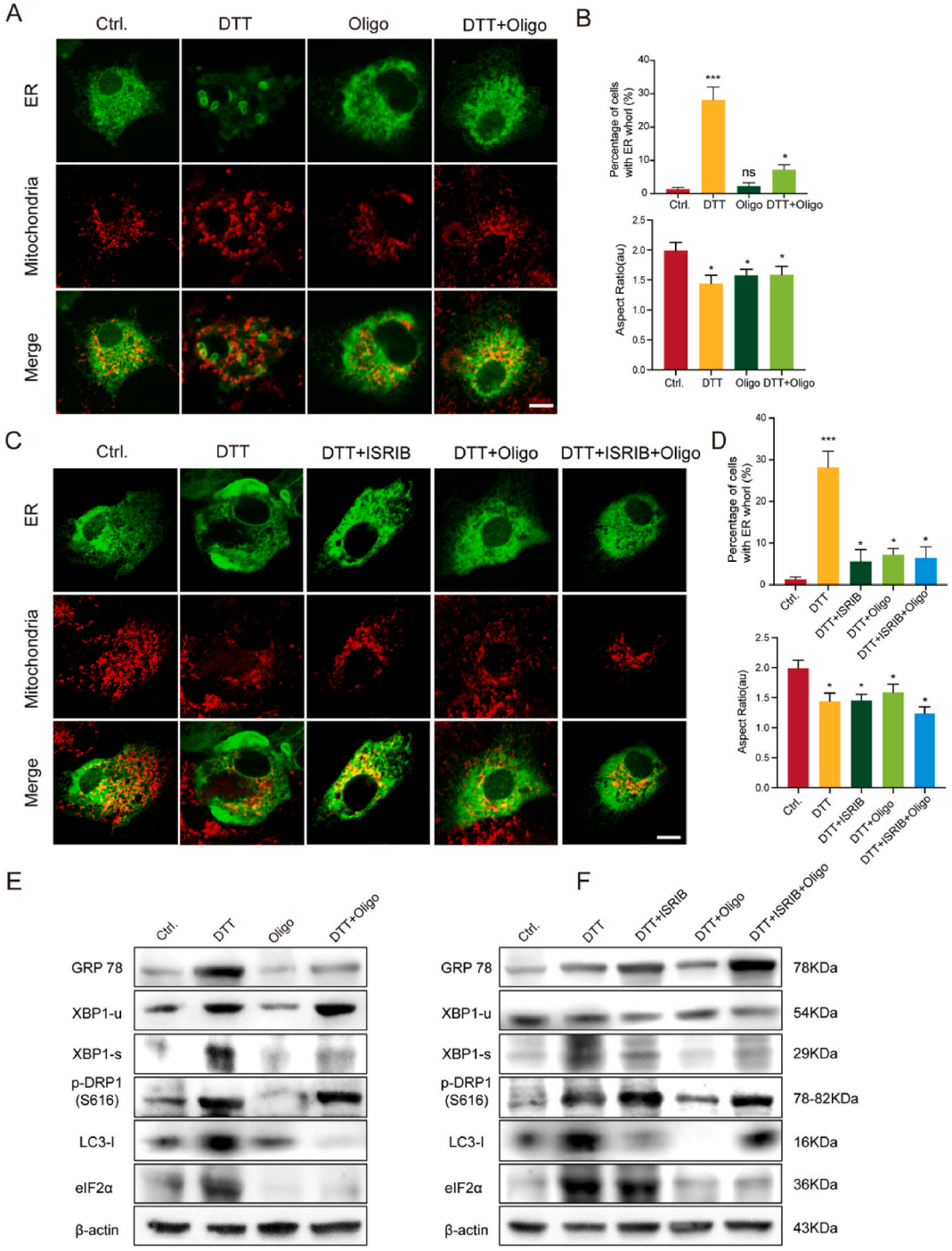

(caption on next page)

Fig. 5. Eukaryotic translation initiation factor (eIF)-2α integrates the stress responses of multiple organelles to regulate atherosclerotic plaque progression. **(A)** Representative image of ER labeled with GFP-Sec61β and mitochondria stained with deep red Mitotracker in HC-VSMCs treated with DMSO (Ctrl.), thapsigargin (Tg; 5 μM), Oligo (1 μM), and combined Tg and oligo for 24 h. **(B)** Quantitative analysis of the percentage of cells with ER whorls and the aspect ratio in HC-VSMCs treated with DMSO (Ctrl.), Tg, Oligo, and combined Tg and Oligo (n = 30 cells per group). **(C)** Representative image of ER labeled with GFP-Sec61β and mitochondria stained with deep red Mitotracker in HC-VSMCs treated with DMSO (Ctrl.), Tg (5 μM), ISRIB (100 nM), Oligo (1 μM), and their combination for 24 h. **(D)** Quantitative analysis of the percentage of cells with ER whorls and the aspect ratio in HC-VSMCs treated with DMSO, DTT, ISRIB, Oligo, and their combination (n = 30 cells per group). **(E)** Western blotting analysis of GRP78, XBP1-u, XBP1-s, p-DRP1(S616), LC3-I, and eIF2α in HC-VSMCs treated with DMSO (Cntrl.), Tg, Oligo, and combined Tg and Oligo (n = 3 in each group). **(F)** Western blotting analysis of GRP78, XBP1-u, XBP1-s, p-DRP1(S616), LC3-I, and eIF2α in HC-VSMCs treated with DMSO, Tg, ISRIB, Oligo, and their combination (n = 3 times each group). *p < 0.05, **p < 0.01, and ***p < 0.001. Scale bar = 10 μm. (For interpretation of the references to colour in this figure legend, the reader is referred to the Web version of this article.)

We explored whether eIF2α mediated ISR functions in atherosclerosis. Firstly,the expression of eIF2α was dramatically upregulated and downregulated under ER stress and mitochondrial stress, respectively, implying the diversed role of ER stress and mitochondria stress targeting eIF2α (Fig. 5E; Supplementary Figure 2D). Next, we used ISRIB, an eIF2α phosphorylation inhibitor, to further confirm the role of eIF2α in regulating ISR. Similar to oligomycin A, ISRIB also blocked the formation of ER whorls induced by Tg, and concomitant treatment with oligomycin A and ISRIB did not cause further ER whorl reduction, implying that mitochondrial stress may function through eIF2α to alleviate ER stress (Fig. 5C and D). Consistently, western blotting showed reduced XBP-1 splicing and autophagy after a combination of Tg and ISRIB (Fig. 5F; Supplementary Figure 2E). As ISRIB is a specific phosphorylation inhibitor of eIF2α, eIF2α did not change at the protein expression level (Fig. 5F; Supplementary Figure 2E). However, both eIF2α phosphorylation inhibition (ISRIB) and expression suppression (mitochondrial stress induced by oligomycin A) are active in rescuing the ER whorl phenomenon, UPR activation, and autophagy, implying that both phosphorylation and abundance of eIF2α are important for ISR. These findings verify the core role of eIF2α in ER and mitochondrial stress. Elevated eIF2α is a critical factor for reducing ER and mitochondrial stress, which eventually regulates lysosome-mediated autophagy.

4. Discussion

In this study, we observed differences between various cellular organelles derived from stable and vulnerable human carotid plaques. Primary VSMCs derived from vulnerable plaques exhibit more severe morphological alterations in ER whorls, fragmented mitochondria, and enlarged lysosomes than primary VSMCs derived from stable plaques. In terms of the mechanism, we found that changes in organelles caused by atherosclerotic stimulation were accompanied by a change in the expression of eIF2α, which suggests that eIF2α may be a common regulator for integrating these organelle stresses (Fig. 6).

It has become increasingly apparent that VSMCs are crucial for initiating, developing, and stabilizing atherosclerosis [38]. Primary cells are receiving increasing recognition in cell biology, particularly in fields such as oncology and cardiovascular research [39]. We found that primary VSMCs derived from vulnerable plaques exhibit more morphological and functional alterations in ER stress, mitochondrial stress, and lysosomal defects than those derived from stable plaques. Based on these results, we mimicked the atherosclerotic environment with high glucose and ox-LDL in VSMCs cell lines. In contrast, the results of the quantitative analysis revealed that established VSMCs treated with atherosclerotic stimulation could not perfectly reproduce the organelle changes detected in primary VSMCs derived from stable and vulnerable plaques. These results indicated the superiority of primary VSMCs for exploring the molecular mechanisms of atherosclerosis as well as the complexity of atherosclerosis. Thus, primary VSMCs derived from human plaques may be a reliable tool for reflecting the complexity of atherosclerosis. However, the identification and monitoring of VSMC differentiation remain challenging. Thus, future research is required to define the phenotype during the isolation of VSMCs is still needed.

eIF2α is an essential translation-initiating regulatory protein that determines the expression of multiple protein synthesis [40]. The

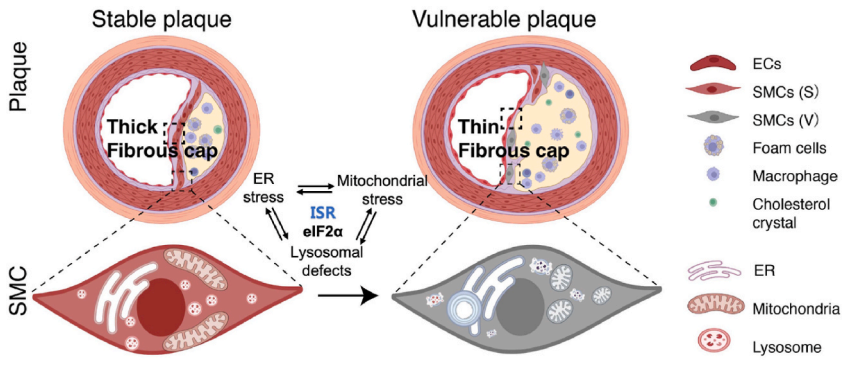

Fig. 6. Schematic representation of the changes in organelles associated with ER stress, mitochondrial stress, and lysosomal defects between stable and vulnerable plaques, and the eIF2α-mediated those integrated stress responses.

phosphorylation of eIF2α is a response to various stress stimuli, which locks eIF2 in its inactive form, thereby reducing protein synthesis and favoring the metabolic dormancy required for cell survival under stress. Conversely, non-phosphorylated eIF2α increased protein synthesis and promoted cell proliferation. Increasing evidence has shown that eIF2α is an important translation hub that participates in cell proliferation and survival, malignant transformation, tumor initiation, progression, and metastasis [41]. In our study, we found that eIF2α participates in a variety of organelle stresses, such as ER stress, mitochondrial stress, and lysosomal defects. Previous studies have demonstrated that the PERK-eIF2α signaling pathway regulates ER stress, followed by an altered degree of autophagy or apoptosis [42]. In addition, several studies have reported that eIF2α phosphorylation is essential for inducing reactive oxygen species generation from dysfunctional mitochondria [43]. However, only a few studies have reported the integrated role of eIF2α in ISR. Interestingly, we discovered the integrated role of eIF2α in organelle stress in VSMCs and carotid plaques, which may be a potential target for regulating cellular stress, thereby alleviating atherosclerotic progression. However, the detailed interaction between eIF2α and organelle stress merits further investigation.

5. Conclusion

In this study, we found that dysregulated organelle dynamics in primary VSMCs may serve as a practical clue to the pathological mechanisms of atherosclerosis. We also found that eIF2α-mediated ISR is a crucial regulator of atherosclerosis development at the subcellular level, indicating its potential as a novel therapeutic target for the treatment of atherosclerotic carotid stenosis.

Funding

This study was supported by the Beijing Science and Technologic Project (Z201100005520020), National Natural Science Foundation of China (grant 82171303), and Beijing Municipal Science &Technology Commission (No. 5202022).

Ethics approval and consent to participate

Our study complied with the Declaration of Helsinki and was approved by the hospital ethical review board (Xuanwu Hospital, Capital Medical University, Beijing, China). The informed written consent was obtained from all patients.

Availability of data and materials

All data will be shared upon reasonable request to the corresponding author. The datasets used and/or analyzed during the current study are available from the corresponding author on reasonable request.

CRediT authorship contribution statement

Jichang Luo: Writing – review & editing, Writing – original draft, Methodology, Data curation. **Xiao Zhang:** Data curation. **Wenjing Li:** Methodology, Conceptualization. **Tao Wang:** Supervision, Methodology. **Shengyan Cui:** Formal analysis, Data curation. **Tianhua Li:** Formal analysis. **Yilin Wang:** Methodology. **Wenlong Xu:** Formal analysis. **Yan Ma:** Supervision. **Bin Yang:** Visualization, Validation. **Yumin Luo:** Validation. **Ge Yang:** Supervision, Conceptualization. **Ran Xu:** Writing – review & editing, Supervision. **Liqun Jiao:** Writing – review & editing, Supervision, Conceptualization.

Declaration of competing interest

The authors declare the following financial interests/personal relationships which may be considered as potential competing interests: Liqun Jiao reports financial support was provided by the Beijing Science and Technologic Project (Z201100005520020), National Natural Science Foundation of China (grant 82171303), and Beijing Municipal Science &Technology Commission (No. 5202022). No reports a relationship with The authors report no disclosures relevant to the manuscript. that includes: funding grants. No has patent licensed to Liqun Jiao. The authors report no disclosures relevant to the manuscript. If there are other authors, they declare that they have no known competing financial interests or personal relationships that could have appeared to influence the work reported in this paper.

Acknowledgements

A preprint has previously been published [1].

Appendix A. Supplementary data

Supplementary data related to this article can be found at https://doi.org/10.1016/j.heliyon.2024.e26904.

References

[1] J. Luo, X. Zhang, W. Li, T. Wang, Y. Wu, T. Li, et al., eIF2α Mediated Integrated Stress Response Connects Multiple Intracellular Signaling to Reprogram Vascular Smooth Muscle Cell Fate in Carotid Plaques, 2022, https://doi.org/10.21203/rs.3.rs-2022646/v1. PREPRINT (Version 1).
[2] M.L. Flaherty, B. Kissela, J.C. Khoury, K. Alwell, C.J. Moomaw, D. Woo, et al., Carotid artery stenosis as a cause of stroke, Neuroepidemiology 40 (2013) 36–41.
[3] W. Brinjikji, J. Huston 3rd, A.A. Rabinstein, G.M. Kim, A. Lerman, G. Lanzino, Contemporary carotid imaging: from degree of stenosis to plaque vulnerability, J. Neurosurg. 124 (2016) 27–42.
[4] B. Yang, Y. Ma, T. Wang, Y. Chen, Y. Wang, Z. Zhao, et al., Carotid endarterectomy and stenting in a Chinese population: safety outcome of the revascularization of extracranial carotid artery stenosis trial, Transl Stroke Res 12 (2021) 239–247.
[5] G.L. Basatemur, H.F. Jorgensen, M.C.H. Clarke, M.R. Bennett, Z. Mallat, Vascular smooth muscle cells in atherosclerosis, Nat. Rev. Cardiol. 16 (2019) 727–744.
[6] X. Bi, C. Du, X. Wang, X.Y. Wang, W. Han, Y. Wang, et al., Mitochondrial damage-induced innate immune activation in vascular smooth muscle cells promotes chronic kidney disease-associated plaque vulnerability, Adv. Sci. 8 (2021) 2002738.
[7] E. Di Pasquale, G. Condorelli, Endoplasmic reticulum stress at the crossroads of progeria and atherosclerosis, EMBO Mol. Med. 11 (2019).
[8] H.C.F. Oliveira, A.E. Vercesi, Mitochondrial bioenergetics and redox dysfunctions in hypercholesterolemia and atherosclerosis, Mol. Aspect. Med. 71 (2020) 100840.
[9] A. Misra, Z. Feng, R.R. Chandran, I. Kabir, N. Rotllan, B. Aryal, et al., Integrin beta3 regulates clonality and fate of smooth muscle-derived atherosclerotic plaque cells, Nat. Commun. 9 (2018) 2073.
[10] Z. Zhang, P. Yue, T. Lu, Y. Wang, Y. Wei, X. Wei, Role of lysosomes in physiological activities, diseases, and therapy, J. Hematol. Oncol. 14 (2021) 79.
[11] R. Heald, O. Cohen-Fix, Morphology and function of membrane-bound organelles, Curr. Opin. Cell Biol. 26 (2014) 79–86.
[12] Q. Ba, G. Raghavan, K. Kiselyov, G. Yang, Whole-cell scale dynamic organization of lysosomes revealed by spatial statistical analysis, Cell Rep. 23 (2018) 3591–3606.
[13] W. Li, S. Zhang, G. Yang, Dynamic organization of intracellular organelle networks, WIREs Mechanisms of Disease 13 (2020).
[14] I. Çimen, B. Kocatürk, S. Koyuncu, Ö. Tufanlı, U.I. Onat, A.D. Yıldırım, et al., Prevention of atherosclerosis by bioactive palmitoleate through suppression of organelle stress and inflammasome activation, Sci. Transl. Med. 8 (2016), 358ra126-358ra126.
[15] N. Donnelly, A.M. Gorman, S. Gupta, A. Samali, The eIF2α kinases: their structures and functions, Cell. Mol. Life Sci. 70 (2013) 3493–3511.
[16] N. Burwick, B.H. Aktas, The eIF2-alpha kinase HRI: a potential target beyond the red blood cell, Expert Opin. Ther. Targets 21 (2017) 1171–1177.
[17] M.J. Clemens, Initiation factor eIF2α phosphorylation in stress responses and apoptosis, Signaling Pathways for Translation (2001) 57–89.
[18] A.R. Naylor, P.M. Rothwell, P.R. Bell, Overview of the principal results and secondary analyses from the European and North American randomised trials of endarterectomy for symptomatic carotid stenosis, Eur. J. Vasc. Endovasc. Surg. 26 (2003) 115–129.
[19] M. Naghavi, P. Libby, E. Falk, S.W. Casscells, S. Litovsky, J. Rumberger, et al., From vulnerable plaque to vulnerable patient: a call for new definitions and risk assessment strategies: Part I, Circulation 108 (2003) 1664–1672.
[20] M.J. Zhang, Y. Zhou, L. Chen, Y.Q. Wang, X. Wang, Y. Pi, et al., An overview of potential molecular mechanisms involved in VSMC phenotypic modulation, Histochem. Cell Biol. 145 (2016) 119–130.
[21] I. Murashov, A. Volkov, G. Kazanskaya, E. Kliver, A. Chernyavsky, D. Nikityuk, et al., Immunohistochemical features of different types of unstable atherosclerotic plaques of coronary arteries, Bull. Exp. Biol. Med. 166 (2018) 102–106.
[22] L. Liao, Q. Zhou, Y. Song, W. Wu, H. Yu, S. Wang, et al., Ceramide mediates Ox-LDL-induced human vascular smooth muscle cell calcification via p38 mitogen-activated protein kinase signaling, PLoS One 8 (2013) e82379.
[23] B.S. Jhun, H. Lee, Z.G. Jin, Y. Yoon, Glucose stimulation induces dynamic change of mitochondrial morphology to promote insulin secretion in the insulinoma cell line INS-1E, PLoS One 8 (2013) e60810.
[24] R. Virmani, F.D. Kolodgie, A.P. Burke, A. Farb, S.M. Schwartz, Lessons from sudden coronary death: a comprehensive morphological classification scheme for atherosclerotic lesions, Arterioscler. Thromb. Vasc. Biol. 20 (2000) 1262–1275.
[25] Y. Guo, D. Shen, Y. Zhou, Y. Yang, J. Liang, Y. Zhou, et al., Deep learning-based morphological classification of endoplasmic reticulum under stress, Front. Cell Dev. Biol. 9 (2021) 767866.
[26] F. Xu, W. Du, Q. Zou, Y. Wang, X. Zhang, X. Xing, et al., COPII mitigates ER stress by promoting formation of ER whorls, Cell Res. 31 (2021) 141–156.
[27] J.J. Greenfield, S. High, The Sec61 complex is located in both the ER and the ER-Golgi intermediate compartment, J. Cell Sci. 112 (Pt 10) (1999) 1477–1486.
[28] S.B. Berman, F.J. Pineda, J.M. Hardwick, Mitochondrial fission and fusion dynamics: the long and short of it, Cell Death Differ. 15 (2008) 1147–1152.
[29] A. Ballabio, J.S. Bonifacino, Lysosomes as dynamic regulators of cell and organismal homeostasis, Nat. Rev. Mol. Cell Biol. 21 (2020) 101–118.
[30] C. Chi, A.S. Riching, K. Song, Lysosomal abnormalities in cardiovascular disease, Int. J. Mol. Sci. 21 (2020).
[31] A.R.A. Marques, C. Ramos, G. Machado-Oliveira, O.V. Vieira, Lysosome (Dys)function in atherosclerosis-A big weight on the shoulders of a small organelle, Front. Cell Dev. Biol. 9 (2021) 658995.
[32] M.E. de Araujo, G. Liebscher, M.W. Hess, L.A. Huber, Lysosomal size matters, Traffic 21 (2020) 60–75.
[33] L. Edgar, N. Akbar, A.T. Braithwaite, T. Krausgruber, H. Gallart-Ayala, J. Bailey, et al., Hyperglycemia induces trained immunity in macrophages and their precursors and promotes atherosclerosis, Circulation 144 (2021) 961–982.
[34] S. Allahverdian, C. Chaabane, K. Boukais, G.A. Francis, M.L. Bochaton-Piallat, Smooth muscle cell fate and plasticity in atherosclerosis, Cardiovasc. Res. 114 (2018) 540–550.
[35] W. Zhou, J.D. Faraldo-Gómez, Membrane plasticity facilitates recognition of the inhibitor oligomycin by the mitochondrial ATP synthase rotor, Biochimica et Biophysica Acta (BBA)-Bioenergetics 1859 (2018) 789–796.
[36] R. Emanuel, I. Sergin, S. Bhattacharya, J.N. Turner, S. Epelman, C. Settembre, et al., Induction of lysosomal biogenesis in atherosclerotic macrophages can rescue lipid-induced lysosomal dysfunction and downstream sequelae, Arterioscler. Thromb. Vasc. Biol. 34 (2014) 1942–1952.
[37] C. Mauvezin, T.P. Neufeld, Bafilomycin A1 disrupts autophagic flux by inhibiting both V-ATPase-dependent acidification and Ca-P60A/SERCA-dependent autophagosome-lysosome fusion, Autophagy 11 (2015) 1437–1438.
[38] M.O.J. Grootaert, M.R. Bennett, Vascular smooth muscle cells in atherosclerosis:Time for a reassessment, Cardiovasc. Res. 117 (2021) 2326–2339.
[39] M.M. Davidson, C. Nesti, L. Palenzuela, W.F. Walker, E. Hernandez, L. Protas, et al., Novel cell lines derived from adult human ventricular cardiomyocytes, J. Mol. Cell. Cardiol. 39 (2005) 133–147.
[40] Y.K. Tao, P.L. Yu, Y.P. Bai, S.T. Yan, S.P. Zhao, G.Q. Zhang, Role of PERK/eIF2α/CHOP endoplasmic reticulum stress pathway in oxidized low-density lipoprotein mediated induction of endothelial apoptosis, Biomed. Environ. Sci. 29 (2016) 868–876.
[41] S.R. Kimball, Eukaryotic initiation factor eIF2, Int. J. Biochem. Cell Biol. 31 (1999) 25–29.
[42] T. Zhang, D. Li, L. Wan, X. Chen, X. Wang, B. Zhong, et al., Ctenopharyngodon idella PERK (EIF2AK3) decreases cell viability by phosphorylating eIF2α under ER stress, Fish Shellfish Immunol. 70 (2017) 568–574.
[43] B.M. Baker, A.M. Nargund, T. Sun, C.M. Haynes, Protective coupling of mitochondrial function and protein synthesis via the eIF2α kinase GCN-2, PLoS Genet. 8 (2012) e1002760.